Biometals (2009) 22:733–751
DOI 10.1007/s10534-009-9221-8

# Crystal structures, antioxidation and DNA binding properties of Yb(III) complexes with Schiff-base ligands derived from 8-hydroxyquinoline-2-carbaldehyde and four aroylhydrazines

**Yong-chun Liu · Zheng-yin Yang**

Received: 4 January 2009 / Accepted: 6 February 2009 / Published online: 25 February 2009


**Abstract** X-ray crystal and other structural analyses indicate that Yb(III) and all four newly synthesized ligands can form a binuclear Yb(III) complex with a 1:1 metal to ligand stoichiometry by octacoordination at the Yb(III) center. Investigations of DNA binding properties show that all the ligands and Yb(III) complexes can bind to Calf thymus DNA through intercalations with the binding constants at the order of magnitude $10^5$–$10^7$ $M^{-1}$, but Yb(III) complexes present stronger affinities to DNA than ligands. All the ligands and Yb(III) complexes may be used as potential anticancer drugs. Investigations of antioxidation properties show that all the ligands and Yb(III) complexes have strong scavenging effects for hydroxyl radicals and superoxide radicals but Yb(III) complexes show stronger scavenging effects for hydroxyl radicals than ligands.

**Electronic supplementary material** The online version of this article (doi:10.1007/s10534-009-9221-8) contains supplementary material, which is available to authorized users.

Y.-c. Liu · Z.-y. Yang (✉)
State Key Laboratory of Applied Organic Chemistry, College of Chemistry and Chemical Engineering, Lanzhou University, 730000 Lanzhou, People's Republic of China
e-mail: yangzy@lzu.edu.cn; ychliu001@163.com

Y.-c. Liu
College of Chemistry and Chemical Engineering, Longdong University, 745000 Qingyang, Gansu, People's Republic of China

**Keywords** Rare earths · Schiff bases · X-ray crystallography · Calf thymus DNA binding properties · Antioxidation

## Introduction

DNA is an important cellular receptor, many chemicals exert their antitumor effects through binding to DNA thereby changing the replication of DNA and inhibiting the growth of the tumor cells, which is the basis of designing new and more efficient antitumor drugs and their effectiveness depends on the mode and affinity of the binding (Zeng et al. 2003; Pyle et al. 1990; Barton et al. 1986). A number of metal chelates, as agents for mediation of strand scission of duplex DNA and as chemotherapeutic agents, have been used as probes of DNA structure in solution (Mahadevan and Palaniandavar 1997; Lippard 1978; Hecht 1986). Apart from the magnetic and photophysical properties, the bioactivities of lanthanides such as antimicrobial, antitumor, antivirus, anticoagulant action, enhancing NK and Macrophage cell activities, prevention from arteriosclerosis, etc., have been explored in recent decades (Parker et al. 2002; Albrecht et al. 2005; Hunter and Walker 1956; Kramsch et al. 1981). In addition, Schiff bases are able to inhibit the growth of several animal tumors, and some metal chelates have shown good antitumor activities against animal tumors (Hodnett and Mooney

1970; Hodnett and Dunn 1972). So, well designed organic ligands enable a fine tuning of special properties of the metal ions. The chemistry of quinoline and its derivatives has also attracted special interest due to their therapeutic properties. Quinoline sulphonamides have been used in the treatment of cancer, tuberculosis, diabetes, malaria, and convulsion (Schmidt 1969; El-Asmy et al. 1990). Albrecht and coworkers reported that both the crystal structures of $[YLNO_3)(DMF)_2]_2Cl_2{\cdot}2(DMF)$ and $[LaL(NO_3)(MeOH)_2]_2(NO_3)_2$ with nonacoordination have central planar four-membered $(LaO)_2$ and $(YbO)_2$ rings, respectively, where ligand L-H is 2-[(8-hydroxyquinolinyl)methylene]hydrazinecarboxamide and acts as a tetradentate ligand binding to yttrium(III) and lanthanum(III) (Albrecht et al. 2005). Such structures may have strong affinities of binding to DNA through intercalations. In this paper, four Schiff-base ligands, structurally similar to the ligand L-H, were prepared from 8-Hydroxyquinoline-2-carbaldehyde with four aroylhydrazines to form their ytterbium(III) complexes and to investigate the DNA binding properties.

On the other hand, an excess of activated oxygen species in the forms of superoxide anion ($O_2^{-\cdot}$) and hydroxyl radical ($OH^{\cdot}$), generated by normal metabolic processes, may cause various diseases such as carcinogenesis, drug-associated toxicity, inflammation, atherogenesis, and aging in aerobic organisms (Ames et al. 1993; Horton and Fairhurst 1987; Wang et al. 2006). Although the naturally occurring antioxidants can scavenge free radicals in the body, they have been limited by their low effectiveness even though they are considered to be active in eliminating reactive oxygen and controlling toxic effects. The potential value of antioxidants has prompted investigators to search for the cooperative effects of metal complexes and natural compounds for improving antioxidant activity and cytotoxicity (Lo et al. 2004). It has been recently demonstrated that some minor groove binders for DNA are effective inhibitors of the formation of a DNA/TBP complex or topoisomerases (Chiang et al. 1994; Woynarowski et al. 1989; Chen et al. 1993). Adding a reactive entity endowed with oxidative properties should improve the efficiency of inhibitors. The antioxidation properties of the ligands and Yb(III) complexes were investigated in this paper. Furthermore, the substituent effects of these compounds on antioxidation and DNA binding properties were investigated further.

## Materials and methods

### Materials

Calf thymus DNA (CT-DNA) and Ethidium bromide (EtBr) were obtained from Sigma–Aldrich Biotech. Co., Ltd. 8-Hydroxyquinoline-2-carbaldehyde was obtained form J&K Chemical Co., Ltd. All the stock solutions (1.0 mmol) of the investigated compounds were prepared by dissolving the powder materials into appropriate amounts of DMF solutions, respectively. Deionized double distilled water and analytical grade reagents were used throughout. CT-DNA stock solution was prepared by dissolving the solid material, normally at 0.3 mg $ml^{-1}$, in 5 mmol Tris–HCl buffer (pH 7.20) containing 50 mmol NaCl. Then, the solution was kept over 48 h at 4°C. The resulting somewhat viscous solution was clear and particle-free. The solution of CT-DNA in Tris–HCl buffer gave a ratio of UV–vis absorbance at 260–280 nm of about 1.8–1.9, indicating that the CT-DNA was sufficiently free of protein. The CT-DNA concentration in terms of base pair $L^{-1}$ was determined spectrophotometrically by employing an extinction coefficient of $\varepsilon = 13{,}200$ $M^{-1}$ $cm^{-1}$ (base pair)$^{-1}$ at 260 nm. The CT-DNA concentration in terms of nucleotide $L^{-1}$ was also determined spectrophotometrically by employing an extinction coefficient of 6,600 $M^{-1}$ $cm^{-1}$ (nucleotide)$^{-1}$ at 260 nm (Zsila et al. 2004). The stock solution was stored at −20°C until it was used. Working standard solution of CT-DNA was obtained by appropriate dilution of the stock solution in 5 mmol Tris–HCl buffer (pH 7.20) containing 50 mmol NaCl. EtBr was dissolved in 5 mmol Tris–HCl buffer (pH 7.20) and its concentration was determined assuming a molar extinction coefficient of 5,600 l $mol^{-1}$ $cm^{-1}$ at 480 nm (Suh and Chaires 1995).

### Methods

The melting points of the compounds were determined on an XT4-100X microscopic melting point apparatus (Beijing, China). Elemental analyses of C, N and H were carried out on an Elemental Vario EL analyzer. The metal ion content was determined by complexometric titration with EDTA after destruction of the complex in the conventional manner. The IR spectra were recorded on a Nicolet Nexus 670 FT-IR spectrometer using KBr disc in the 4,000–400 $cm^{-1}$

regions. $^1$H NMR spectra were recorded on a Bruker Avance DRX 200-MHz spectrometer with tetramethylsilane (TMS) as an internal standard. ESI-MS (ESI-Trap/Mass) spectra were recorded on a Bruker Esquire6000 Mass spectrophotometer. Ultraviolet–visible (UV–vis) spectra were obtained using a PerkinElmer Lambda UV–vis spectrophotometer.

Viscosity titration experiments were carried on an Ubbelohde viscometer in a thermostated water-bath maintained at 25.00 ± 0.01°C. Titrations were performed for an investigated compound that was introduced into DNA solution (50 μM, bps) present in the viscometer. Data were presented as $(\eta/\eta_o)^{1/3}$ versus the ratio of the compound to DNA, where $\eta$ is the viscosity of DNA in the presence of the compound corrected from the solvent effect, and $\eta_o$ is the viscosity of DNA alone. Relative viscosities for DNA in either the presence or absence of compound were calculated from the following relation (Suh and Chaires 1995; Satyanarayana et al. 1992):

$$\eta = (t - t_o)/t_o \tag{1}$$

where $t$ is the observed flow time of the DNA containing solution, and $t_o$ is the flow time of buffer.

Fluorescence spectra were recorded using RF-5301PC spectrofluorophotometer (Shimadzu, Japan) with a 1 cm quartz cell. Both of the excitation and emission band widths were 10 nm. All the experiments were measured after 5 min at a constant room temperature, 298 K. The intrinsic binding constants $K_b$ could be obtained by the fluorescence titration methods and Scatchard equation (Scatchard 1949):

$$r/\mathrm{C}_f = nK_b - rK_b \tag{2}$$

where $r$ is the moles of compound bound per mole nucleotides of DNA; $C_f$ is the molar concentration of free compound; $n$ is the number of binding sites or the maximum number of compound bound per nucleotide, and $K_b$ is the association or binding constant. $C_f$ and $r$ could be calculated according to the following equations (Wang et al. 2007):

$$C_f = C_t - C_b \tag{3}$$

$$C_b = C_t(F - F_o)/(F_{\max} - F_o) \tag{4}$$

$$r = C_b/C_{DNA} \tag{5}$$

where $C_t$ is the total molar concentration of compound; $C_b$ is the molar concentration of compound bound for DNA; $F$ is the observed fluorescence emission intensity at a given DNA concentration $C_{\mathrm{DNA}}$ (nucleotides); $F_o$ is the fluorescence emission intensity in the absence of DNA; and $F_{\max}$ is the maximum fluorescence emission intensity of the compound totally bound for DNA at a titration end point. The binding constants were also obtained by McGhee and von Hippel model (Chaires et al. 1982; McGhee and von Hippel 1974):

$$\frac{r}{C_f} = K_b(1 - nr)\left[\frac{1 - nr}{1 - (n-1)r}\right]^{n-1} \tag{6}$$

where $K_b$ is the intrinsic binding constant and $n$ is the exclusion parameter in DNA base pairs. The experimental parameters $K_b$ and $n$ were adjusted to produce curves that gave, by inspection, the most satisfactory fits to the experimental data.

EtBr–DNA quenching assay was performed as reported in a literature but with small changes (Krishna et al. 1998). DNA (4.0 μM, nucleotides) solution was added incrementally to 0.32 μM EtBr solution, until the rise in the fluorescence ($\lambda_{\mathrm{ex}} = 496$ nm, $\lambda_{\mathrm{em}} = 596$ nm) attained a saturation. Then, small aliquots of concentrated compound solutions (1.0 mmol) were added till the drop in fluorescence intensity ($\lambda_{\mathrm{ex}} = 525$ nm, $\lambda_{\mathrm{em}} = 587$ nm) reached a constant value. Measurements were made after 5 min at a constant room temperature, 298 K. Stern-Volmer equation was used to determine the fluorescent quenching mechanisms (Suh and Chaires 1995):

$$F_o/F = 1 + K_q\tau_o[Q] = 1 + K_{SV}[Q] \tag{7}$$

where $F_o$ and $F$ are the fluorescence intensity in the absence and in the presence of a compound at $[Q]$ concentration, respectively; $K_{SV}$ is the Stern–Volmer dynamic quenching constant; $K_q$ is the quenching rate constant of bimolecular diffusion collision; $\tau_o$ is the lifetime of free EtBr.

The hydroxyl radicals in aqueous media were generated through the Fenton-type reaction (Winterbourn 1981, 1979). The 5 ml reaction mixtures contained 2.0 ml of 100 mmol phosphate buffer (pH = 7.4), 1.0 ml of 0.10 mmol aqueous safranin, 1 ml of 1.0 mmol aqueous EDTA–Fe(II), 1 ml of 3% aqueous $H_2O_2$, and a series of quantitatively microadding solutions of the tested compound. The sample without the tested compound was used as the control. The reaction mixtures were incubated at 37°C for 60 min in a water-bath. Absorbance at 520 nm was measured and the solvent effect was

corrected throughout. The scavenging effect for $OH^{\cdot}$ was calculated from the following expression (Wang et al. 2007; Guo et al. 2005):

$$\text{Scavenging effect (\%)} = \frac{A_{\text{sample}} - A_{\text{blank}}}{A_{\text{control}} - A_{\text{blank}}} \times 100 \quad (8)$$

where $A_{\text{sample}}$ is the absorbance of the sample in the presence of the tested compound, $A_{\text{blank}}$ is the absorbance of the blank in the absence of the tested compound and $A_{\text{control}}$ is the absorbance in the absence of the tested compound and EDTA–Fe(II).

The superoxide radicals ($O_2^{-\cdot}$) were produced by the MET–Vit$B_2$–NBT system (Wang et al. 2007; Guo et al. 2005). The solution of MET (methionine), Vit$B_2$ (vitamin $B_2$), and NBT (nitroblue tetrazolium) were prepared with deionized double distilled water under lightproof conditions. The 5 ml reaction mixtures contained 2.5 ml of 100 mmol phosphate buffer (pH 7.8), 1.0 ml of 50 mmol MET, 1.0 ml of 0.23 mmol NBT, 0.50 ml of 33 μM Vit$B_2$, and a series of quantitatively microadding solutions of the tested compound. After incubated at 30°C for 10 min in a water-bath and then illuminated with a fluorescent lamp (4000 Lux), the absorbance of the sample was measured at 560 nm and the solvent effect was corrected throughout. The sample reaction mixtures without the tested compound were used as the control. The scavenging effect for $O_2^{-\cdot}$ was calculated from the following expression:

$$\text{Scavenging effect (\%)} = \frac{A_o - A_i}{A_o} \times 100 \quad (9)$$

where $A_i$ is the absorbance in the presence of the tested compound, $A_o$ is the absorbance in the absence of the tested compound. The data for antioxidation presented as means ± SD of three determinations and followed by Student's *t*-test. Differences were considered to be statistically significant if $P < 0.05$. $IC_{50}$ value was introduced to denote the molar concentration of the tested compound which caused a 50% inhibitory or scavenging effect on hydroxyl radicals or superoxide radicals.

Synthesis of 8-hydroxyquinoline-2-carbaldehyde-(benzoyl)hydrazone (**1a**, $H_2L^1$)

Ligand **1a** was prepared by refluxing and stirring a 10 ml ethanol solution of 8-hydroxyquinoline-2-carbaldehyde (0.519 g, 3 mmol) and a 10 ml 90% ethanol aqueous solution of benzoylhydrazine (0.408 g, 3 mmol) for 8 h. After cooling to room temperature, the precipitate was filtered, recrystallized from 80% methanol aqueous solution and dried in vacuum over 48 h to give a pale yellow powder, yield 74.7% (0.652 g). m.p. = 221°C. ESI-MS *m/z* 292.1 $[M + H]^+$. $^1$H NMR (DMSO-$d_6$, 200 MHz, TMS): 8.637 (s, 1 H, 11-CH = N), 8.343 (d, J = 8.8 Hz, 1 H, 4-CH), 8.119 (d, J = 8.8 Hz, 1 H, 3-CH), 7.936 (d, J = 6.4 Hz, 2 H, 16,20-CH), 7.630–7.507 (m, 3 H, 17,18,19-CH), 7.467–7.387 (m, 2 H, 5,6-CH), 7.131 (d, 1 H, J = 5.0 Hz, 7-CH). IR (KBr): 3,359, 3,318, 1,682, 1,602, 1,546, 1,267 $cm^{-1}$.

Synthesis of 8-hydroxyquinoline-2-carbaldehyde-(2′-hydroxybenzoyl)hydrazone (**1b**, $H_2L^2$)

Ligand **1b**, a yellow precipitate, was obtained from equimolar amounts of 8-hydroxyquinoline-2-carbaldehyde and 2-hydroxybenzoylhydrazine in the same way as ligand **1a**. Yield 81.0% (0.746 g). m.p. = 245–247°C. ESI-MS *m/z* 308.2 $[M + H]^+$. $^1$H NMR (DMSO-$d_6$, 200 MHz, TMS): 8.621 (s, 1 H, 11-CH = N), 8.356 (d, J = 8.6 Hz, 1 H, 4-CH), 8.113 (d, J = 8.6 Hz, 1 H, 3-CH), 7.871 (d, 1 H, J = 7.8 Hz, 20-CH), 7.469–7.395 (m, 3 H, 5,6, 18-CH), 7.133 (d, J = 7.0 Hz, 1 H, 7-CH), 7.018–6.943 (m, 2 H, 17,19-CH). IR (KBr): 3,464, 3,250, 1,643, 1,607, 1,532, 1,288 $cm^{-1}$.

Synthesis of 8-hydroxyquinoline-2-carbaldehyde-(4′-hydroxybenzoyl)hydrazone (**1c**, $H_2L^3$)

Ligand **1c**, a pale yellow precipitate, was obtained from equimolar amounts of 8-hydroxyquinoline-2-carbaldehyde and 4-hydroxybenzoylhydrazine similar to ligand **1a**. Yield 84.2% (0.776 g). m.p. = 279–280°C. ESI-MS *m/z* 308.2 $[M + H]^+$. $^1$H NMR (DMSO-$d_6$, 200 MHz, TMS): 8.594 (s, 1 H, 11-CH = N), 8.329 (d, J = 8.4 Hz, 1 H, 4-CH), 8.088 (d, J = 8.4 Hz, 1 H, 3-CH), 7.834 (d, 2 H, J = 10.4 Hz, 16,20-CH), 7.493–7.379 (m, 2 H, 5,6-CH), 7.124 (d, J = 6.8 Hz, 1 H, 7-CH), 6.900 (d, J = 10.4 Hz, 2 H, 17,19-CH). IR (KBr): 3,320, 3,139, 1,660, 1,632, 1,581, 1,277 $cm^{-1}$.

Synthesis of 8-hydroxyquinoline-2-carbaldehyde-(isonicotinyl)hydrazone (**1d**, $H_2L^4$)

Ligand **1d**, a yellow precipitate, was also obtained from equimolar amounts of 8-hydroxyquinoline-2-carbaldehyde and isonicotinylhydrazine in the same way as **1a**. Yield 71.0% (0.622 g). m.p. = 162–164°C. ESI-MS *m/z* 293.2 $[M + H]^+$. $^1H$ NMR (DMSO-$d_6$, 200 MHz, TMS): 8.813 (d, J = 5.2 Hz, 2 H, 17,19-CH), 8.657 (s, 1 H, 11-CH = N), 8.372 (d, J = 8.8 Hz, 1 H, 4-CH), 8.129 (d, J = 8.8 Hz, 1 H, 3-CH), 7.861 (d, J = 5.2 Hz, 2 H, 16,20-CH), 7.528–7.409 (m, 2 H, 5,6-CH), 7.148 (d, J = 6.4 Hz, 1 H, 7-CH). IR (KBr): 3,576, 3,193, 1,663, 1,613, 1,557, 1,271 $cm^{-1}$.

Synthesis of complex **2a**

Complex **2a** was prepared by refluxing and stirring equimolar amounts of a 40 ml methanol solution of ligand **1a** (0.058 g, 0.2 mmol) and $Yb(NO_3)\cdot 6H_2O$ on a water-bath. After refluxed for 30 min, triethylamine (0.020 g, 0.2 mmol) was added into the reaction mixtures dropwise to deprotonate the phenolic hydroxyl substituent of 8-hydroxyquinolinato unit. Then, the mixtures were refluxed and stirred continuously for 8 h. After cooling to room temperature, the precipitate was centrifugalized, washed with methanol and dried in vacuum over 48 h to give an orange powder, yield 87.2% (0.101 g). Anal. calcd. for $C_{37}H_{33}N_9O_{13}Yb_2$: C 38.35, H 2.85, N 10.88, Yb 29.89. found: C 38.29, H 2.84, N 10.90, Dy 29.84. ESI-MS *m/z* 1,364.2 $[M + Na]^+$ (DMF solution). IR (KBr): 3,412, 1,606, 1,555, 1,493, 1,310, 1,106, 1,029, 946, 841, 741, 615, 567, 495 $cm^{-1}$. Λm (DMF) = 40.9 $cm^2\ \Omega^{-1}\ mol^{-1}$.

Synthesis of complex **2b**

Similarly, complex **2b** was prepared from equimolar amounts of $Yb(NO_3)\cdot 6H_2O$ and **1b**. Yield: 88.4% (0.105 g). Anal. calcd. for $C_{37}H_{33}N_9O_{15}Yb_2$: C 37.32, H 2.77, N 10.59, Yb 29.09. found: C 37.28, H 2.77, N 10.60, Dy 29.04. ESI-MS *m/z* 1,396.3 $[M + Na]^+$ (DMF solution). IR (KBr): 3,385, 3,193, 1,602, 1,549, 1,499, 1,305, 1,261, 1,103, 1,031, 972, 836, 753, 675, 576, 496 $cm^{-1}$. Λm (DMF) = 46.0 $cm^2\ \Omega^{-1}\ mol^{-1}$.

Synthesis of complex **2c**

Complex **2c** was prepared from equimolar amounts of $Yb(NO_3)\cdot 6H_2O$ and **1c**. Yield: 91.6% (0.109 g). Anal. calcd. for $C_{37}H_{33}N_9O_{15}Yb_2$: C 37.32, H 2.77, N 10.59, Yb 29.09. found: C 37.32, H 2.77, N 10.57, Dy 29.13. ESI-MS *m/z* 1,396.3 $[M + Na]^+$ (DMF solution). IR (KBr): 3,422, 3,186, 1,600, 1,542, 1,490, 1,291, 1,240, 1,107, 1,082, 976, 844, 766, 637, 560, 491 $cm^{-1}$. Λm (DMF) = 37.9 $cm^2\ \Omega^{-1}\ mol^{-1}$.

Synthesis of complex **2d**

Complex **2d** was prepared from equimolar amounts of $Yb(NO_3)\cdot 6H_2O$ and **1d**. Yield: 82.8% (0.960 g). Anal. calcd. for $C_{35}H_{31}N_{11}O_{13}Yb_2$: C 36.22, H 2.67, N 13.28, Yb 29.84. found: C 36.29, H 2.67, N 13.30, Dy 29.90. ESI-MS *m/z* 1,366.2 $[M + Na]^+$ (DMF solution). IR (KBr): 3,387, 1,635, 1,594, 1,551, 1,489, 1,315, 1,103, 1,060, 937, 844, 753, 616, 570, 493 $cm^{-1}$. Λm (DMF) = 44.8 $cm^2\ \Omega^{-1}\ mol^{-1}$.

Determination of crystal structures

X-ray diffraction data for a crystal were performed with graphite-monochromated Mo $K\alpha$ radiation (0.71073 Å) on a Bruker APEX area-detector diffractometer and collected by the $\omega$-$2\theta$ scan technique at 296(2) K. The crystal structure was solved by direct methods. All non-hydrogen atoms were refined anisotropically by full-matrix least-squares methods on $F^2$. A partial structure was obtained by direct methods and the remaining non-hydrogen atoms were located from difference maps. Hydrogen atoms were located in geometrically defined positions and not refined. All calculations were performed using the programs SHELXS-97 and SHELXL-97 (Sheldrick 1990).

## Results and discussion

Chemical syntheses of ligands and Yb(III) complexes

Four Schiff-base ligands, 8-hydroxyquinoline-2-carbaldehyde-(benzoyl)hydrazone (**1a**, $H_2L^1$), 8-hydroxyquinoline-2-carbaldehyde-(2′-hydroxybenzoyl)hydrazone

(**1b**, $H_2L^2$), 8-hydroxyquinoline-2-carbaldehyde-(4′-hydroxybenzoyl)hydrazone (**1c**, $H_2L^3$) and 8-hydroxyquinoline-2-carbaldehyde-(isonicotinyl)hydrazone (**1d**, $H_2L^4$) were prepared from equimolar amounts of 8-hydroxyquinoline-2-carbaldehyde and benzoylhydrazine, 2-hydroxybenzoylhydrazine, 4-hydroxybenzoylhydrazine, and isonicotinylhydrazine, respectively. Their structures were determined by IR spectroscopy, $^1$H NMR and ESI-MS. The synthetic routes for ligands are presented in Scheme 1. Then, the Yb(III) complexes (**2a-d**) were easily prepared from these ligands and equimolar amounts of $Yb(NO_3)\cdot 6H_2O$, respectively.

## Crystal structure analyses of the Yb(III) complexes

The orange transparent, X-ray quality crystals of complex **2b** and **2d** were obtained by vapor diffusion of diethyl ether into DMF solution of the powdered complex at room temperature for 2 weeks. Crystal data and structure refinements for the X-ray structural analyses are presented in Table 1. Selected bond lengths and angles of the metal complexes are presented in Table S1 and Table S2 (see Supplementary data Table S1–S2).

## The crystal structure of complex **2b**

The complex **2b**, formula $C_{46}H_{50}N_{12}O_{16}Yb_2$, crystallizes with a dimension of 0.27 × 0.25 × 0.20 mm in the triclinic system, space group $P\bar{1}$, with lattice parameters $a = 9.9897(6)$ Å, $b = 10.0063(6)$ Å, $c = 14.3543(9)$ Å, $\alpha = 69.6110(10)°$, $\beta = 76.3310(10)°$, $\gamma = 78.1080(10)°$, $F(000) = 678$, GOF = 0.996, $R_1 = 0.0234$, $wR_2 = 0.0564$, $Z = 1$. $D_{calc} = 1.761$ g cm$^{-3}$, $V = 1{,}294.75(14)$ Å$^3$. The coordination sphere of ORTEP diagram (30% probability ellipsoids) in Fig. 1a shows that the complex composition is of $[YbL^2(NO_3)(DMF)]_2\cdot(DMF)$. Ligand **1b** acts as a dibasic tetradentate ligand, binding to $Yb^{3+}$ through the phenolate oxygen atom, nitrogen atom of quinolinato unit and the C = N group, $^-$O–C = N– group (enolized and deprotonated from O = C–NH–) of the 2–hydroxybenzoylhydrazine side chain. One DMF molecule is binding orthogonal to the ligand-plane from one side to the metal ion, while one nitrate (bidentate) is binding from another. Dimerization of this monomeric unit occurs through the phenolate oxygen atoms leading to a central four-membered $(YbO)_2$ ring with a Yb···Yb separation of 3.7238(4) Å. At the dimerization site, a "set off" of the two parallel "$YbL^2$-planes" by 1.258 Å takes place. Moreover, there is a free DMF solvent molecule in the lattice. The space group for structure of complex **2b** is $P\bar{1}$. This space group has a center of symmetry. The calculated density is 1.761 g cm$^{-3}$, which indicates that only one dimeric molecule is present in the unit cell, which in turn means that the dimeric complex must have a center of symmetry in the crystal structure (Chen and Cai 2003). This center of symmetry according to the coordinates is at 1/2, 1/2, 0. It is located in the middle of the four-membered $(YbO)_2$ ring formed by the two Yb atoms and the phenolic oxygen atoms. Because of the center of symmetry this four-membered $(YbO)_2$ ring should be planar and the bond angles for the ring indicates this to be the case as shown in Table 2 and Table S1 (see Supplementary data Table S1). Another result of the fact that the dimeric molecule has a center of symmetry is that the two least-squares planes through the two ligands (**1b**) will be parallel (1.258 Å). The

**Scheme 1** The synthetic routes for ligands (**1a–d**)

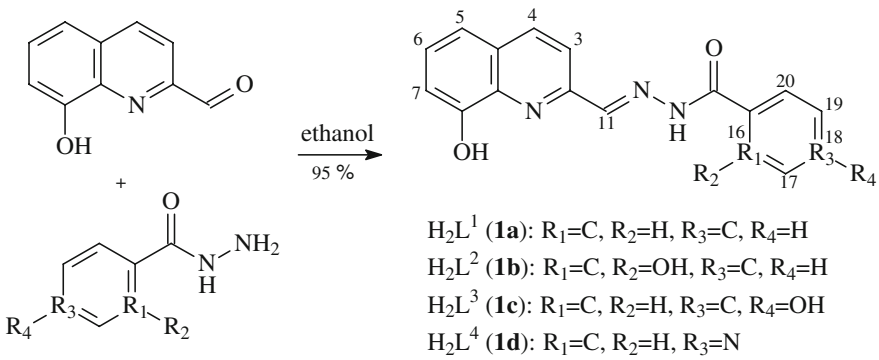


$H_2L^1$ (**1a**): $R_1$=C, $R_2$=H, $R_3$=C, $R_4$=H
$H_2L^2$ (**1b**): $R_1$=C, $R_2$=OH, $R_3$=C, $R_4$=H
$H_2L^3$ (**1c**): $R_1$=C, $R_2$=H, $R_3$=C, $R_4$=OH
$H_2L^4$ (**1d**): $R_1$=C, $R_2$=H, $R_3$=N

**Table 1** Crystal data and structure refinement of metal complexes

| Complex | $[YbL^2(NO_3)(DMF)]_2 \cdot (DMF)$ | $[YbL^4(NO_3)(DMF)]_2 \cdot (DMF)$ |
|---|---|---|
| CCDC deposition number | 713873 | 713874 |
| Chemical formula | $C_{46}H_{50}N_{12}O_{16}Yb_2$ | $C_{44}H_{48}N_{14}O_{14}Yb_2$ |
| Formula weight | 1,373.06 | 1,343.04 |
| Crystal colour | Orange | Orange |
| Crystal size (mm) | 0.27 × 0.25 × 0.20 | 0.31 × 0.27 × 0.23 |
| $T$ (K) | 296(2) | 296(2) |
| Wavelength (Å) | 0.71073 | 0.71073 |
| Radiation | Mo Kα | Mo Kα |
| Crystal system | Triclinic | Orthorhombic |
| Space group | $P\bar{1}$ | *Pbca* |
| $Z$ | 1 | 4 |
| $a$ (Å) | 9.9897(6) | 20.002(3) |
| $b$ (Å) | 10.0063(6) | 11.4645(17) |
| $c$ (Å) | 14.3543(9) | 22.675(3) |
| $\alpha$ (°) | 69.6110(10) | 90 |
| $\beta$ (°) | 76.3310(10) | 90 |
| $\gamma$ (°) | 78.1080(10) | 90 |
| $V$ (Å$^3$) | 1,294.75(14) | 5,199.8(13) |
| $D$ (calc) (g cm$^{-3}$) | 1.761 | 1.716 |
| $\mu$ (mm$^{-1}$) | 3.670 | 3.651 |
| $F$(000) | 678 | 2,648 |
| $\theta_{min/max}$ (°) | 1.54–25.05 | 2.04–25.38 |
| Index ranges | $-10 \leq h \leq 11$, | $-24 \leq h \leq 23$, |
| | $-11 \leq k \leq 11$, | $-13 \leq k \leq 13$, |
| | $-17 \leq l \leq 16$ | $-23 \leq l \leq 27$ |
| Reflections collected | 6,532 | 25,726 |
| Independent reflections | 4,508 ($R_{int} = 0.0168$) | 4,755 ($R_{int} = 0.1112$) |
| Absorption correction | Semi-empirical from equivalents | Semi-empirical from equivalents |
| Max. and min. transmission | 0.5273 and 0.4374 | 0.438 and 0.336 |
| Refinement method | Full-matrix least-squares on $F^2$ | Full-matrix least-squares on $F^2$ |
| Data/restraints/parameters | 4,508/0/349 | 4,755/0/338 |
| Goodness-of-fit on $F^2$ | 0.996 | 1.051 |
| Final $R$ indices [$I > 2\sigma$ ($I$)] | $R_1 = 0.0234$, $wR_2 = 0.0564$ | $R_1 = 0.0517$, $wR_2 = 0.1060$ |
| $R$ indices (all data) | $R_1 = 0.0269$, $wR_2 = 0.0579$ | $R_1 = 0.1122$, $wR_2 = 0.1334$ |
| $\rho_{min/max}$ (e Å$^{-3}$) | 1.098 and −0.766 | 1.673 and −1.511 |

bonded DMF molecule, the non-bonded DMF molecule and the bonded nitrate are thus also related by a center of symmetry to the respective moieties in the other half of the dimeric molecule. Their thermal parameters are rather large due to this fact. In addition, this crystal structure of the binuclear complex with a 1:1 metal to ligand stoichiometry by octacoordination is similar to that of $[YL(NO_3)(DMF)_2]_2Cl_2 \cdot 2(DMF)$ or $[LaL(NO_3)(MeOH)_2]_2(NO_3)_2$, where ligand L-H is 2-[(8-hydroxyquinolinyl)methylene]hydrazinecarboxamide and acts as a monad tetradentate ligand binding to $Y^{3+}$ or $La^{3+}$ through the phenolate oxygen atom, nitrogen atom of quinolinato unit and the C = N group, C = O group of the

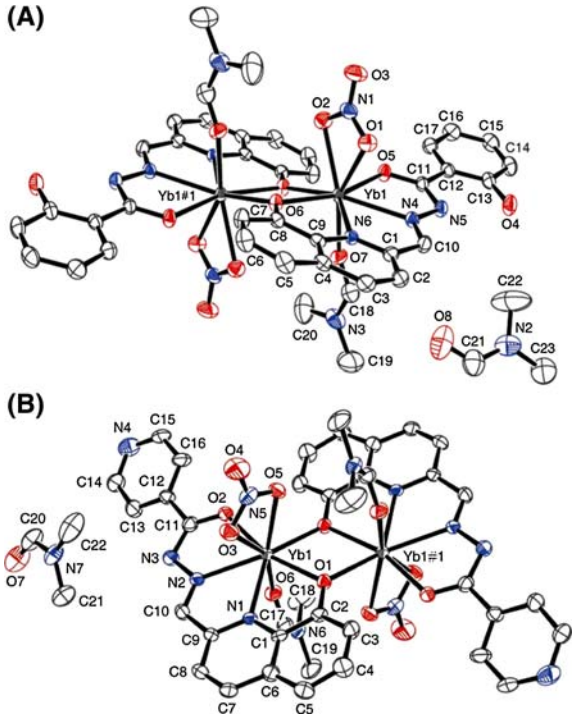


**Fig. 1** Coordination spheres of ORTEP diagrams (30% probability ellipsoids) of $[YbL^2(NO_3)(DMF)_2]_2$ (**a**) and $[YbL^4(NO_3)(DMF)_2]_2$ (**b**) complexes

semicarbazone side chain (Albrecht et al. 2005). However, there are some marked differences between them as shown in Table 2. The first, the "set off" of the two parallel "$YbL^2$-planes" by 1.258 Å takes place while the "set off" of the two parallel "YL-planes" and "LaL-planes" by accurately 1.887 (CCDC 273601) and 1.388 Å (CCDC 273600) take place, respectively, though they were reported by approximately 2 Å. The second, this crystal structure of binuclear complex is a 1:1 metal to ligand stoichiometry by octacoordination but $[YL(NO_3)(DMF)_2]_2Cl_2{\cdot}2(DMF)$ or $[LaL(NO_3)(MeOH)_2]_2(NO_3)_2$ complex is a 1:1 metal to ligand stoichiometry by nonacoordination. This is due to the fact that in the present structure only one DMF molecule is coordinated to $Yb^{3+}$ and in those of Albrecht both DMF molecules are coordinated to $Y^{3+}$ or $La^{3+}$. The third, O = C–NH– group of the 2-hydroxybenzoylhydrazine side chain has enolized and deprotonated into $^{-}$O–C = N– group after the formation of $[YbL^2(NO_3)(DMF)]_2{\cdot}(DMF)$ complex, where the C–$O^{-}$ band length is 1.279(4) Å and the N = C double band length is 1.333(5) Å. The normal band lengths of C = O, C–N, C–O and C = N are 1.19–1.23, 1.47–1.50, 1.30–1.39 and 1.34–1.38 Å, respectively (Chen and Cai 2003).

**Table 2** Comparison of the structural parameters of ligand L–H (Albrecht et al. 2005), ligand **1b** and **1d** when binding to different metal centers

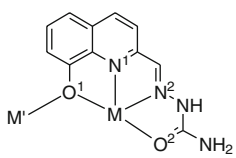


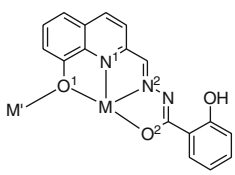


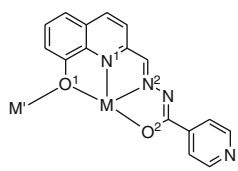


| | $[LY(NO_3)(DMF)_2]_2Cl_2{\cdot}2(DMF)$ | $[LLa(NO_3)(MeOH)_2]_2(NO_3)_2$ | $[YbL^2(NO_3)(DMF)]_2{\cdot}(DMF)$ | $[YbL^4(NO_3)(DMF)]_2{\cdot}(DMF)$ |
|---|---|---|---|---|
| O1–M | 2.346(3) | 2.425(3) | 2.315(2) | 2.341(7) |
| N1–M | 2.470(3) | 2.541(3) | 2.393(3) | 2.401(7) |
| N2–M | 2.563(4) | 2.620(4) | 2.452(3) | 2.435(8) |
| O2–M | 2.355(3) | 2.414(3) | 2.244(2) | 2.254(7) |
| O1–M′ | 2.354(3) | 2.387(3) | 2.281(2) | 2.309(7) |
| O1–M–N1 | 66.8(1) | 65.5(1) | 68.10(9) | 67.7(3) |
| N1–M–N2 | 61.4(1) | 60.4(1) | 64.39(9) | 64.3(3) |
| N2–M–O2 | 63.1(1) | 60.9(1) | 64.62(9) | 64.4(3) |
| Distance between the two parallel ML-planes | 1.887 | 1.388 | 1.258 | 1.044 |
| Distance between M···M′ | 3.886 | 3.980 | 3.7238(4) | 3.7553(9) |

Whereas carbonyl group C = O of the semicarbazone side chain has not enolized in $[YL(NO_3)(DMF)_2]_2Cl_2 \cdot 2(DMF)$ or $[LaL(NO_3)(MeOH)_2]_2(NO_3)_2$ complex. The difference in the enolization may well be due to the fact that the organic ligand in the case of the Albrecht structures is cationic, while it is neutral in the present structure and this will be investigated in the future study. The deprotonization difference is therefore a result of the way the organic ligand was synthesized. However, carbonyl group C = O directly linking with aromatic group may be favourable of enolizing under the present experimental conditions, so as to form a larger conjugated and a lower energy system, than the non-aromatic group such as $–NH_2$ when binding to metal ion and forming a complex. It is the enolization and deprotonation of O = C–NH– group changing into $^{-}$O–C = N– that the $[YbL^2(NO_3)(DMF)]_2 \cdot (DMF)$ complex is of neutral charge and non-electrolyte, but both of $[YL(NO_3)(DMF)_2]_2Cl_2 \cdot 2(DMF)$ and $[LaL(NO_3)(MeOH)_2]_2(NO_3)_2$ complexes are of electrolytes. The enolization and deprotonation will afford an efficient route for investigators to design favorable molecules well. On the other hand, the 2-hydroxyl substituent linking with benzoylhydrazine has not take part in binding to $Yb^{3+}$, largely due to the steric effect and long distance (5.172 Å) between the 2-hydroxyl substituent and $Yb^{3+}$, but it may form an intra-molecular hydrogen band, a stabilizing six-membered ring, with adjacent nitrogen atom (1.847 Å) of the same side chain.

## The crystal structure of complex **2d**

The complex **2d**, formula $C_{44}H_{48}N_{14}O_{14}Yb_2$, crystallizes with dimensions 0.31 × 0.27 × 0.23 mm in the orthorhombic system, space group *Pbca*, with lattice parameters $a = 20.002(3)$ Å, $b = 11.4645(17)$ Å, $c = 22.675(3)$ Å, $\alpha = 90°$, $\beta = 90°$, $\gamma = 90°$, $F(000) = 2{,}648$, GOF = 1.051, $R_1 = 0.0517$, $wR_2 = 0.1060$, $Z = 4$. $D_{calc} = 1.716$ g cm$^{-3}$, $V = 5{,}199.8(13)$ Å$^3$. The coordination sphere of ORTEP diagram (30% probability ellipsoids) in Fig. 1b shows that the complex composition is of $[YbL^4(NO_3)(DMF)]_2 \cdot (DMF)$. The crystal of the binuclear complex with a 1:1 metal to ligand stoichiometry by octacoordination is much similar to that of $[YbL^2(NO_3)(DMF)]_2 \cdot (DMF)$. Ligand **1d** also acts as a dibasic tetradentate ligand, binding to $Yb^{3+}$ through the phenolate oxygen atom, nitrogen atom of quinolinato unit and the C = N group, $^{-}$O–C = N– group (enolized and deprotonated from O = C–NH–) of the isonicotinylhydrazine side chain, where the $^{-}$O–C and N = C band lengths are 1.269(12) and 1.334(13) Å, respectively. One DMF molecule is binding orthogonal to the ligand-plane from one side to the metal ion, while one nitrate (bidentate) is binding from another. Similarly, there is a free DMF solvent molecule in the lattice. Dimerization of this monomeric unit also occurs through the phenolate oxygen atoms leading to a central planar four-membered $(YbO)_2$ ring with a Yb···Yb separation of 3.7553(9) Å. At the dimerization site, a "set off" of two parallel "$YbL^4$-planes" by 1.044 Å takes place. On the basis of 4 moleculles per unit cell the density is calculated to be 1.716 g cm$^{-3}$. The space group *Pbca* has 8 asymmetric units, therefore the dimeric molecules needs to be located on a center of symmetry. The coordinate shows the center of symmetry is at 0, 1/2, 1. Thus the central 4-membered $(YbO)_2$ ring is planar and the planes through the two ligands are parallel (1.044 Å) as in the complex **2b**. The distance between the two parallel ML-planes and M···M' as shown in Table 2 may result from the size of $M^{3+}$ and substituent effects simultaneously.

On the other hand, there are a number of B and C Alerts in the CIF/PLATON reports for crystal structures of the metal complexes, which are largely due to the crystal qualities, but they are not significant in the understanding of crystal structure determinations.

## Elemental analysis and molar conductance for powder metal complexes

All the Yb(III) complexes are of orange powders, stable in air, and soluble in DMF and DMSO, but slightly soluble in methanol, ethanol, acetonitrile, ethyl acetate and acetone, THF and $CHCl_3$. The melting points of all the Yb(III) complexes exceed 300°C. Elemental analyses indicate that all the Yb(III) complexes are of 1:1 metal to ligand (stoichiometry) complexes, and the data of molar conductance of the Yb(III) complexes in DMF solutions indicate that all of them act as non-electrolytes (Geary 1971).

## Infrared spectrum study for powder metal complexes

In comparison with the characteristic IR bands of 8-hydroxyquinoline-2-carbaldehyde, the characteristic IR spectrum bands ($\nu_{max}/cm^{-1}$) of all the ligands showed $3{,}576–3{,}320_{vs}$ assigned to $\nu$(NH); $1{,}682–1{,}643_{s}$ assigned to $\nu$(CO) of the carbonyl groups of aroylhydrazine side chains and 1,632–1,602 assigned to $\nu$(CN) of azomethines, whereas $1{,}706_{s}$ assigned to $\nu$(CO) of the formyl disappeared. Moreover, $3{,}318–3139_{br}$ and $1{,}288–1{,}267_{s}$ should be assigned to $\nu$(OH) and $\nu$(C–OH) of the phenolic hydroxyl substituents, respectively, and 1,581–1,532 should be assigned to $\nu$(CN) of pyridines. Carefully compared with the characteristic IR bands of ligands, it comes to the conclusion that: (1) All the complexes show $3{,}422–3{,}385_{br}$ assigned to $\nu$(OH) of $H_2O$; $976–937_{w}$ assigned to $\rho_r$ ($H_2O$) and $675–615_{w}$ assigned to $\rho_w$ ($H_2O$), indicating that there are coordinated water molecules participating in the Yb(III) complexes (Moawad and Hanna 2002; Ismail 2005). (2) All the complexes show 1,107–1,103 assigned to $\nu$(C–OM), indicating that the binding of metal ion to every ligand through an O–M covalent linkage takes place (Ou-Yang 1997). (3) $3{,}318–3{,}139_{s}$ assigned to $\nu$(OH) and 1,288–1,267 assigned to $\nu$(C–OH) of the phenolic hydroxyl substituent of ligands have disappeared, but the new bands of $3{,}193_{s}$ and $1{,}261_{s}$ can be respectively, assigned to $\nu$(OH) and $\nu$(C–OH) of the phenolic hydroxyl substituent of 2-hydroxybenzoylhydrazine side chain of **2b** complex, while the new bands of $3{,}186_{s}$ and $1{,}240_{s}$ can also be respectively, assigned to $\nu$(OH) and $\nu$(C–OH) of the phenolic hydroxyl substituent of 4-hydroxybenzoylhydrazine side chain of **2c** complex. (4) $1{,}682–1{,}643_{s}$ assigned to $\nu$(CO) and $3{,}576–3{,}320_{vs}$ assigned to $\nu$(NH) of aroylhydrazine side chains of ligands have disappeared in all the IR spectra of Yb(III) complexes, indicating that they participate in the Yb(III) complexes with the groups of O = C–NH– of aroylhydrazine side chains enolized and deprotonated into $^{-}$O–C = N– as proved by the above crystal structural analyses. (5) 1,635–1,600 assigned to $\nu$(CN) of azomethines of the Yb(III) complexes have shifted by 32–4 $cm^{-1}$ in comparison with bands of ligands, indicating that the nitrogen atoms of azomethines participate in the complexes. (6) 1,555–1,542 assigned to $\nu$(CN) of pyridines of the Yb(III) complexes have shifted by 39–6 $cm^{-1}$ in comparison with bands of ligands, indicating that the nitrogen atoms of pyridines also participate in the complexes. However, the new band of 1,594 can be assigned to $\nu$(CN) of free pyridine of isonicotinylhydrazine side chain of **2d** complex. (7) $576–560_{w}$ assigned to $\nu$(MO) and $496–491_{w}$ assigned to $\nu$(MN) of the Yb(III) complexes further indicate that oxygen atoms and nitrogen atoms participate in Yb(III) complexes. (8) All the Yb(III) complexes show 1,499–1,489 ($\nu_1$), 1,315–1,291 ($\nu_4$), 1,082–1,029 ($\nu_2$), 844–836 ($\nu_3$), 766–741 ($\nu_5$), and $\Delta\nu(\nu_1–\nu_4) = 199–174$ $cm^{-1}$, indicating that nitrate ions bidentately participate in the Yb(III) complexes (Lu et al. 2006).

Additionally, the ESI-MS data show that the *m/z* ($[M + Na]^+$, DMF solution) are 1,364.2, 1,396.3, 1,396.3 and 1,366.2 for **2a**, **2b**, **2c** and **2d** complexes, respectively, indicating that the two coordinated water molecules for every powder Yb(III) complex can be replaced by two DMF molecules in DMF solution. However, the results of Elemental analyses, molar conductance, IR and ESI-MS data indicate that all the powder metal complexes are structurally similar to each other and their compositions are of $[YbL^{1–4}(NO_3)(H_2O)]_2$.

## Viscosity titration measurements for DNA binding properties

Viscosity titration measurements were carried out to clarify the interaction modes between the investigated compounds and CT-DNA. Viscosity measurements are very sensitive to changes in the length of DNA, as viscosity is proportional to $L^3$ for rod-like DNA of length $L$. Intercalation involves the insertion of a planar molecule between DNA base pairs, which results in a decrease in the DNA helical twist and lengthening of the DNA, therefore intercalators cause the unwinding and lengthening of DNA helix as base pairs become separated to accommodate the binding compound (Suh and Chaires 1995; Palchaudhuri and Hergenrother 2007). Whereas, agents bound to DNA through groove binding do not alter the relative viscosity of DNA, and agents electrostatically bound to DNA will bend or kink the DNA helix, reducing its effective length and its viscosity, concomitantly (Satyanarayana et al. 1992; Wang et al. 2007). The effects of ligands and Yb(III) complexes on the viscosities of CT-DNA are shown in Fig. 2. With the

ratios of the investigated compounds to DNA (bps) increasing, the relative viscosities of DNA increase steadily, indicating that there exist intercalations between all the ligands and Yb(III) complexes with DNA helix. The crystal and other structural analyses show that all the Yb(III) complexes have two parallel planes, which may well be an indicator of the intercalation behaviour of these complexes binding to DNA helix. In addition, although there is a blend at lower molar concentration ratios of complexes to DNA, the relative viscosities of DNA increase with the order of **1a** > **1b** > **1c** > **1d** for ligands, the order of **2a** > **2b** > **2c** > **2d** for Yb(III) complexes, and the orders of **2a** > **1a**, **2b** > **1b**, **2c** > **1c** and **2d** > **1d**.

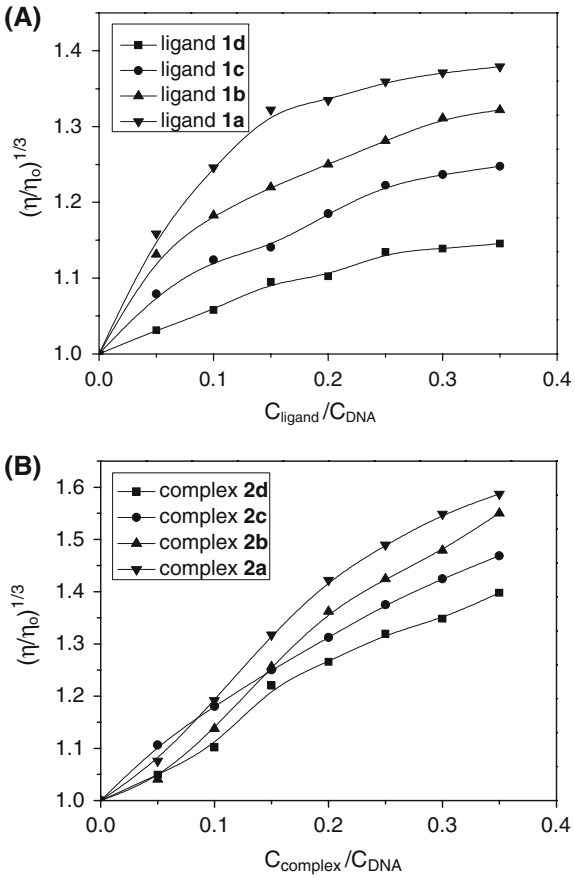


**Fig. 2** Effects of increasing amounts of the investigated compounds on the relative viscosity of CT-DNA in 5 mmol Tris–HCl buffer solution (pH 7.20) containing 50 mmol NaCl at 25.00 ± 0.01°C. Plots of **a** and **b** represent the ligands–CT-DNA and Yb(III) complexes–CT-DNA systems, respectively. The concentration of CT-DNA was 50 μM (bps)

These orders suggest the extents of the unwinding and lengthening of DNA helix by compounds and the affinities of compounds binding to DNA, which may be due to the key roles of substituent effects and the larger coplanar structures of Yb(III) complexes than those of ligands. Intercalation has been traditionally associated with molecules containing fused bi/tricyclic ring structures, though atypical intercalators with nonfused rings systems may be more prevalent than previously recognized (Snyder 2007). So it is logical that all the large coplanar Yb(III) complexes containing fused multiple cyclic ring structures and all the ligands containing fused bicyclic ring structures can bind to DNA through intercalations.

## Ultraviolet–visible (UV–vis) spectroscopy study for DNA binding properties

The UV–vis absorption spectra of the investigated compounds in the absence and in the presence of the CT-DNA were obtained in DMF:Tris–HCl buffer (5 mmol, pH 7.20) containing 50 mmol NaCl of 1:100 solutions, respectively. Data are listed in Table S3 (see Supplementary Data Table S3). The UV–vis spectra of ligands have two types of absorption bands at $\lambda_{max}$ in the regions of 290–300 nm ($\varepsilon = 2.86–3.55 \times 10^4\ M^{-1}\ cm^{-1}$) and 323–329 nm ($\varepsilon = 1.78–2.36 \times 10^4\ M^{-1}\ cm^{-1}$), which can be assigned to $\pi$–$\pi^*$ transitions within the organic molecules, and $\pi$–$\pi^*$ of the C = N and C = O groups, respectively. While the UV–vis spectra of Yb(III) complexes have two types of absorption bands at $\lambda_{max}$ in the regions of 326–334 nm ($\varepsilon = 3.39–4.87 \times 10^4\ M^{-1}\ cm^{-1}$) and 372–379 nm ($\varepsilon = 3.22–4.14 \times 10^4\ M^{-1}\ cm^{-1}$), which can be respectively, assigned to $\pi$–$\pi^*$ transitions of the larger conjugated organic molecules and $\pi$–$\pi^*$ of the C = N–N = C groups coupled with charge transfers from ligands to metal ions ($L \rightarrow Yb^{3+}$) (Moawad and Hanna 2002; Ismail 2005). The band shifts of $\lambda_{max}$ and the changes of $\varepsilon$ for complexes in comparison with ligands indicate the formations of the Yb(III) complexes.

Upon successive additions of CT-DNA (bps), the UV–vis absorption bands of ligand **1a**, **1b**, **1c** and **1d** show a progressive hypochromism of 34.3% at 295 nm, 30.1% at 294 nm, 22.5% at 300 nm and 8.4% at 290 nm by approximately saturated titration end points at $C_{DNA}$:$C_{ligand}$ = 1.4–2.2:1, respectively,

with a 1, 3, 1 and 0 nm red shifts of absorption bands in the region of 290–300 nm. Ligand **1a**, **1b**, **1c** and **1d** show another progressive hypochromism of 11.1% at 323 nm, 18.1% at 329 nm, 4.8% at 326 nm and 1.0% at 325 nm, respectively, with a 1, 3, 1 and 0 nm blue shifts in the region of 323–329 nm. Similarly, upon successive additions of CT-DNA (bps), the UV–vis absorption bands of metal complex **2a**, **2b** and **2c** show a progressive hypochromism of 48.7% at 326 nm, 28.9% at 326 nm and 34.3% at 334 nm by approximately saturated titration end points at $C_{DNA}$:$C_{complex}$ = 1.2–2.0:1, respectively, with 0, 1 and 2 red shifts of absorption bands. Complex **2a**, **2b** and **2c** show another progressive hypochromism of 46.1% at 372 nm, 30.8% at 375 nm and 31.8% at 379 nm, respectively, but all of them show no band shift. Complex **2d** show two types of slightly unsteady hypochromisms of 0.69% at 326 nm with 0 nm band shift and 1.80% at 371 nm with 1 nm red shift by an approximately saturated titration end point at $C_{DNA}$:$C_{complex}$ = 1.4:1. In addition, isosbestic points at 342–357 nm for ligands and at 400–410 nm for Yb(III) complexes are observed, indicating that the reaction between every investigated compound and DNA takes place by an equilibrium. Absorption titration can monitor the interaction of a compound with DNA. The obvious hypochromism and red shift are usually characterized by the noncovalently intercalative binding of compound to DNA helix, due to the strong stacking interaction between the aromatic chromophore of the compound and base pairs of DNA (Barton et al. 1984; Lu et al. 2007). However, the intercalation between a compound and DNA helix can not be excluded only by no or small red shift of UV–vis absorption bands. In fact, some groove binders of Hoechst 33,258 family can also present red shifts or even blue shifts of absorption bands when they bind to DNA helix by groove binding modes, especially for multiple binders (Behrens et al. 2001; Frau et al. 1997). After all, hydrodynamic measurements that are sensitive to length change of DNA (i.e., viscosity and sedimentation) are regarded as the least ambiguous and the most critical criterions for binding modes in solution in absence of crystallographic structural data (Sigman et al. 1993; Wang et al. 2005).

On the other hand, the magnitude of hypochromism is parallel to the intercalative strength and the affinity of a compound binding to DNA (Wu et al. 1997). The appreciable hypochromisms of ligands and Yb(III) complexes intercalating to DNA present the order of **1a** > **1b** > **1c** > **1d** and the order of **2a** > **2c** > **2b** > **2d**. Apart from a slight blend for **2c** and **2d**, these orders are consistent with the viscosity titration results. Here, the substituent effects may play key roles in the interactions. As for complex **2a**, the phenyl substituent may be more accessible to DNA helix and much favorable of forming $\pi$–$\pi$ stacking interaction between the aromatic chromophore of the complex and the base pairs of DNA than 2-hydroxyphenyl and 4-hydroxyphenyl subsituents of **2b** and **2c** complexes. As for complex **2d**, *N* atom of aromatic sextet of the pyridine ring of isonicotinylhydrazine side chain has an exposed and non-hybridized *p* orbital containing two long-pair electrons, which is orthogonal to conjugated $\pi$–$\pi$ plane of the pyridine ring. This may result in a strongly electronic repulsion and hinder the $\pi$–$\pi$ stacking interaction between the aromatic heterocyclic chromophore of the complex and the base pairs of DNA. Moreover, the aggregation of self-stacked molecules of **2d** may occur, which will induces the possibility of an association/dissociation equilibrium in the absence of DNA, and induces a slightly unsteady UV–vis absorption and a little hypochromism even in an excess of conjugate versus DNA bps (Frau et al. 1997). As for the order of hypochromicity for ligands, it may be due to the same reasons as the metal complexes. Difference between them is that no significant aggregation of self-stacked molecules of ligand **1d** may occur unlike complex **2d**.

## EtBr–DNA quenching assay

The fluorescence emission intensity of DNA-EtBr system decreased dramatically upon the increasing amounts of every ligand and Yb(III) complex. Stern–Volmer equation was used to determine the fluorescent quenching mechanism (Suh and Chaires 1995). Plots of $F_o/F$ versus $[Q]$ are shown in Fig. 3 and the quenching data collected and calculated from the good linear relationship when $P < 0.05$ are listed in Table 3. As shown, the data of $K_{SV}$ are 1.405–3.016 $\times$ $10^4$ $M^{-1}$ for ligands and 3.181–15.54 $\times$ $10^4$ $M^{-1}$ for Yb(III) complexes, accordingly, the data of $K_q$ calculated are 0.7806–1.676 $\times$ $10^{13}$ $M^{-1}$ $s^{-1}$ for ligands and 1.767–8.633 $\times$ $10^{13}$ $M^{-1}$ $s^{-1}$ for Yb(III) complexes,

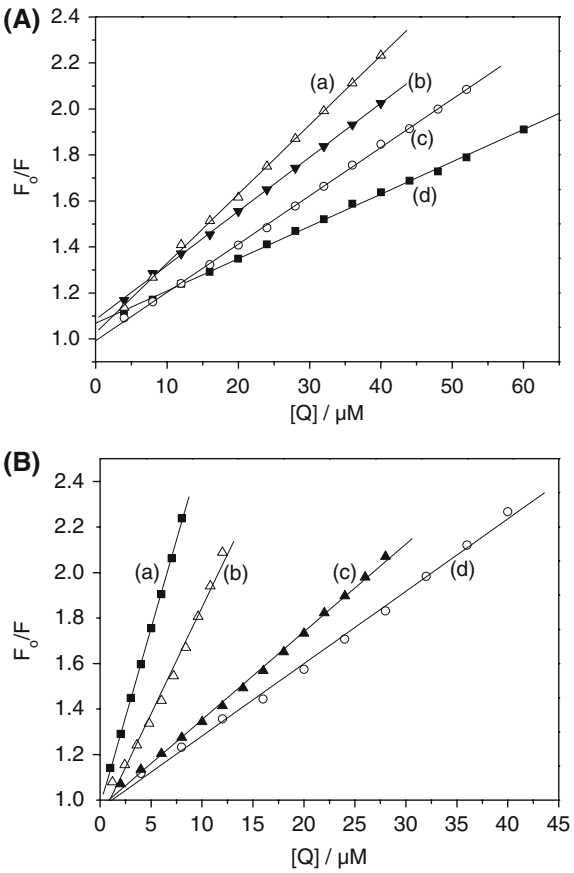


**Fig. 3** Stern–Volmer plots of $F_o/F$ versus [$Q$] for ligands (**a**) and Yb(III) complexes (**b**). Tests were performed in the conditions of 5 mmol Tris–HCl buffer containing 50 mmol NaCl at 298 K. $C_{DNA} = 4$ μM (nucleotides), $C_{EtBr} = 0.32$ μM; $\lambda_{ex} = 525$ nm, $\lambda_{em} = 587$ nm. *Lines* of (*a*), (*b*), (*c*) and (*d*) in plot (**a**) for ligand **1c**, **1b**, **1a** and **1d**, respectively, while *lines* of (*a*), (*b*), (*c*) and (*d*) in plot (**b**) for complex **2c**, **2b**, **2a** and **2d**, respectively

respectively, when the value of $\tau_o$ is taken as $1.8 \times 10^{-9}$ s (Suh and Chaires 1995). All of the current values of $K_q$ for ligands and Yb(III) complexes are much greater than that of $K_{q(max)}$ ($2.0 \times 10^{10}$ $M^{-1}$ $s^{-1}$), the maximum quenching rate constant of bimolecular diffusion collision, which are indicative of static types of quenching mechanisms arisen from the formations of dark complexes between the fluorophores and quenching agents (Liu et al. 2008). It is reported that the loss of fluorescence intensity at the maximum wavelength indicates the displacement of EtBr from DNA–EtBr complex by a compound and the intercalative binding between the compound with

**Table 3** Parameters of $K_b$, $K_{SV}$, $K_q$, $CF_{50}$, $IC_{50}$ (OH and $O_2^-$) for ligands and the Yb(III) complexes ($P < 0.05$)

| Compound | $K_b \times 10^6$ $M^{-1}$ | $1/n$[a] | $K_{SV} \times 10^4$ $M^{-1}$ ($R$) | $K_q \times 10^{13}$ $M^{-1}$ $s^{-1}$ | $CF_{50}$[b] (μM) ($C_{compound}/C_{DNA,\ nucleotides}$) | $IC_{50}$[c] ± SD (μM) for $OH^-$ ($R$) | $IC_{50}$[c] ± SD (μM) for $O_2^-$ ($R$) |
|---|---|---|---|---|---|---|---|
| 1a | 0.2148 ± 0.0205 | 0.081 | 2.086 ± 0.014 (0.9997) | 1.159 | 48.18 (12.05) | 14.66 ± 0.495 (0.9937) | 6.831 ± 0.219 (0.9954) |
| 1b | 0.9295 ± 0.1315 | 0.28 | 2.352 ± 0.018 (0.9998) | 1.307 | 38.95 (9.738) | 7.716 ± 0.230 (0.9940) | 4.308 ± 0.174 (0.9892) |
| 1c | 0.7599 ± 0.0867 | 0.066 | 3.016 ± 0.027 (0.9997) | 1.676 | 32.29 (8.073) | 11.38 ± 0.441 (0.9902) | 4.096 ± 0.112 (0.9955) |
| 1d | 0.1329 ± 0.0180 | 0.092 | 1.405 ± 0.013 (0.9995) | 0.7806 | 66.30 (16.58) | 76.10 ± 0.372 (0.9909) | 5.131 ± 0.258 (0.9838) |
| 2a | 5.624 ± 1.253 | 0.42 | 3.853 ± 0.048 (0.9991) | 2.141 | 26.76 (6.690) | 12.92 ± 0.459 (0.9865) | 7.430 ± 0.255 (0.9950) |
| 2b | 9.320 ± 0.801 | 0.22 | 9.344 ± 0.338 (0.9948) | 5.191 | 11.63 (2.908) | 5.552 ± 0.127 (0.9923) | 7.943 ± 0.519 (0.9762) |
| 2c | 21.78 ± 3.67 | 0.36 | 15.54 ± 0.120 (0.9998) | 8.633 | 6.652 (1.663) | 3.015 ± 0.061 (0.9909) | 31.62 ± 1.85 (0.9913) |
| 2d | 2.506 ± 0.649 | 0.25 | 3.181 ± 0.065 (0.9984) | 1.767 | 32.59 (8.148) | 21.73 ± 0.604 (0.9941) | 12.34 ± 0.514 (0.9940) |

[a] The data of $1/n$ represent moles of compound/mol of base pair of DNA

[b] $CF_{50}$ represents the molar concentration of the tested compound that causes a 50% loss in the fluorescence intensity of EtBr–DNA system

[c] $IC_{50}$ value was calculated from regression line of the log of the tested compound concentration versus the scavenging effect (%) of the compound. $R$ represents the linear correlation coefficient

DNA (Wang et al. 2007). The EtBr–DNA quenching results also indicate that most of the EtBr molecules have been displaced from EtBr–DNA complex by every quencher by the approximately saturated end point. Thus, it is reasonable that there exist intercalations between DNA and these investigated compounds.

Additionally, the Stern–Volmer dynamic quenching constants can also be interpreted as binding affinities of the complexation reactions (Bagatolli et al. 1996; Yang et al. 1994). The data of $K_{SV}$ present the order of **1c** > **1b** > **1a** > **1d** for ligands, the order of **2c** > **2b** > **2a** > **2d** for complexes, and the orders of **2a** > **1a**, **2b** > **1b**, **2c** > **1c**, **2d** > **1d**, which indicate the abilities of displacement of EtBr from EtBr–DNA systems by compounds and the binding affinities between compounds and DNA. However, the orders are not slightly in good agreement with the viscosity titration and UV–vis spectroscopy study results. Here, the phenolic hydroxy groups that can bind to nucleotides or/and the sugar–phosphate backbone of DNA through hydrogen bonds may play certain roles in the EtBr–DNA quenching tests. However, the other weak interactions such as hydrophobic force, Van der Waals force and electrostatic force (pH at 7.20) may not be excluded. In other words, the interaction mechanism is not only determined by complex formation but also by some weak interactions (Ayar and Mercimek 2006).

More importantly, DNA intercalators have been used extensively as antitumor, antineoplastic, antimalarial, antibiotic, and antifungal agents (Suh and Chaires 1995). There is a criterion for screening out antitumor drugs from others by EtBr–DNA fluorescent tracer method, i.e., a compound can be used as potential antitumor drug if it cause a 50% loss of EtBr–DNA fluorescence intensity by fluorescent titrations before the molar concentration ratio of the compound to DNA (nucleotides) does not overrun 100:1 (Li et al. 1991). $CF_{50}$ value is introduced to denote the molar concentration of a compound that causes a 50% loss in the fluorescence intensity of EtBr–DNA system. According to the data of $CF_{50}$ and the molar ratios of compounds to DNA shown in Table 3, it is interesting that at $CF_{50}$, all the molar concentration ratios of the investigated compounds to DNA are largely under 100:1, indicating that all these ligands and Yb(III) complexes can be used as potential antitumor drugs and the antitumor activities of Yb(III) complexes may be better than those of ligands. However, their pharmacodynamical and pharmacological properties should be further studied in vivo.

## Fluorescence spectroscopy study for DNA binding properties

When exited at $\lambda_{ex}$ = 321–325 nm, ligands showed the fluorescence maximum wavelengths at $\lambda_{em}$ = 429–444 nm, and exited at $\lambda_{ex}$ = 327–331 nm the Yb(III) complexes showed the fluorescence maximum wavelengths at $\lambda_{em}$ = 436–441 nm, respectively. Upon additions of DNA, the fluorescence emission intensity of every investigated compound grew steadily. Although the emission enhancement can not be regarded as a rigid criterion for binding mode, it is related to the extent to which the compound gets into a hydrophobic environment inside DNA and avoids the effect of solvent water molecules. To compare quantitatively the affinities of these compounds bound to DNA, the intrinsic binding constants $K_b$ can be obtained by the fluorescence titration methods and Scatchard equation (Scatchard 1949; Wang et al. 2007). Scatchard plot should be a straight line for a simple binding reaction (Berezhkovskiy et al. 2002). Because of the significant neighbour exclusion property of DNA binding to intercalating agents, the Scatchard plot of $r/C_f$ versus $r$ usually presents a deviation from linearity (Chaires et al. 1982). As shown in Fig. S1 (see Supplementary data Fig. S1), every plots of $r/C_f$ versus $r$ for ligands and Yb(III) complexes show deviation from linearity, so the binding constant was obtained by McGhee and von Hippel model (Chaires et al. 1982; McGhee and von Hippel 1974). The data of binding constants ($K_b$) and the moles of compound bound per mol of base pair of DNA ($1/n$) are shown in Table 3. The data of binding constants ($K_b$) present $10^5$ $M^{-1}$ with the order of **1b** > **1c** > **1a** > **1d** for ligands, which is slightly different from the order of EtBr–DNA quenching result. But the data of binding constants ($K_b$) present 2.506–21.78 × $10^6$ $M^{-1}$ with the order of **2c** > **2b** > **2a** > **2d** for complexes, and orders of **2a** > **1a**, **2b** > **1b**, **2c** > **1c**, **2d** > **1d**, which are consistent with the orders of EtBr–DNA quenching results. All the Yb(III) complexes are of stronger binding to DNA in comparison with the classical intercalator (EtBr–DNA, $K_b$ = 3.0 × $10^6$ $M^{-1}$ in 5 mmol Tris–HCl/50 mmol NaCl buffer, pH = 7.2), indicating that the four

Yb(III) complexes can bind to DNA effectively (Baldini et al. 2003).

## Hydroxyl radical scavenging activity

Figure 4a and b show the plots of hydroxyl radical scavenging effect (%) for ligands and Yb(III) complexes, respectively, which are concentration-dependant. As shown in Table 3, the values of $IC_{50}$ of ligands for hydroxyl radical scavenging effect are 7.716–76.10 μM with the order of **1b** < **1c** < **1a** < **1d**, while the values of $IC_{50}$ of Yb(III) complexes for hydroxyl radical scavenging effect are 3.015–21.73 μM with the order of **2c** < **2b** < **2a** < **2d**. These orders of $IC_{50}$ are opposite to the abilities of scavenging effects for hydroxyl radicals. It is marked that the hydroxyl radical scavenging effects of Yb(III) complexes are much higher than those of their ligands, possibly in that the larger conjugated metal complexes can react with $HO^{\cdot}$ to form larger stable macromolecular radicals than ligands (Ueda et al. 1996). Moreover, ligand **1b**, **1c** and their Yb(III) complexes show higher abilities of scavenging effects for hydroxyl radicals than other ligands and Yb(III) complexes, possibly due to the key roles of functional groups, –OH, which can react with $HO^{\cdot}$ to form stable macromolecular radicals by the typical H-abstraction reaction. Furthermore, for hydroxyl radical, there are two types of antioxidation mechanisms, in which one presents suppression of the generation of the

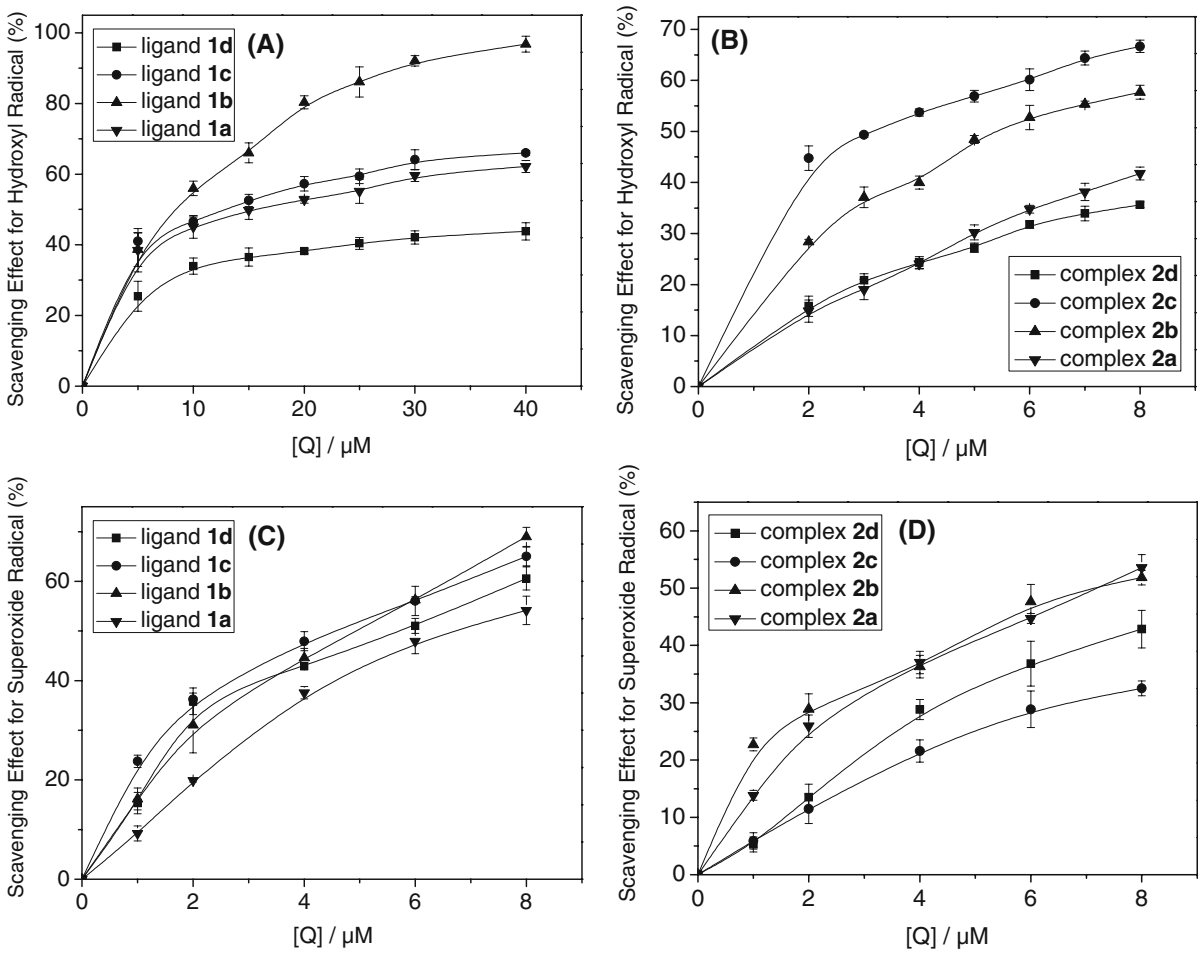


**Fig. 4** Plots of antioxidation properties for ligands and Yb(III) complexes. **a** and **b** represent the hydroxyl radical scavenging effect (%) for ligands and Yb(III) complexes, respectively. **c** and **d** represent the superoxide radical scavenging effect (%) for ligands and Yb(III) complexes, respectively

hydroxyl radicals, and another presents scavenging of the hydroxyl radicals generated (Ueda et al. 1996). Hydroxyl radical production, detected by ethylene formation from methional, has been investigated in plasma, lymph and synovial fluid in the previous study (Winterbourn 1981). In the presence of iron-EDTA as a catalyst, addition of either $H_2O_2$ or xanthine and xanthine oxidase give rise to hydroxyl radical formation that in most cases is not superoxide-dependent. In the absence of iron-EDTA, the reaction is hardly detectable, the rate being less than 5% of that observed with 1 μM iron-EDTA added. In the present study, the chelation between phenolic hydroxyl group and carbonyl group of 2-hydroxybenzoylhydrazine side chain for ligand **1b** with free $Fe^{2+}$ in iron-EDTA reaction system may make the concentration of free $Fe^{2+}$ much lower so that the catalysis becomes very poor and the hydroxyl radical formation has been suppressed, thus, the inhibitive effect of **1b** detected for hydroxyl radical is higher than those of other ligands. However, after formation of Yb(III) complex, the chelation between **1b** and free $Fe^{2+}$ may be destroyed with the formation of intramolecular hydrogen bands for **2b**, so the hydroxyl radical scavenging effect (%) of **2b** is slightly lower than that of complex **2c**.

### Superoxide radical scavenging activity

Figure 4c and d show the plots of superoxide radical scavenging effect (%) for ligands and Yb(III) complexes, respectively, which are also concentration-dependant, but both the plots slightly blend together. As shown in Table 3, the values of $IC_{50}$ of ligands for superoxide radical scavenging effects are 4.096–6.831 μM with no significant difference from each other, but the values of $IC_{50}$ of Yb(III) complexes for superoxide radical scavenging effects are 7.430–31.62 μM with a notably different order of **2a** < **2b** < **2d** < **2c**. These results suggest that there are different mechanisms between scavenging or inhibiting hydroxyl radicals and superoxide radicals, which should be further studied.

It is reported that the value of $IC_{50}$ of ascorbic acid (Vc), a standard agent for non-enzymatic reaction, for hydroxyl radicals is 1.537 mg $ml^{-1}$ (8.727 mmol), and the scavenging effect of Vc for superoxide radicals is only 25% at 1.75 mg $ml^{-1}$ (9.94 mmol; Xing et al. 2005). It is pronounced that all the ligands and the Yb(III) complexes investigated here have much stronger scavenging abilities for hydroxyl radicals and superoxide radicals than ascorbic acid (Vc). Endowed with antioxidative properties, these DNA binders may be effective inhibitors of the formation of a DNA/TBP complex topoisomerases (Chiang et al. 1994; Woynarowski et al. 1989; Chen et al. 1993).

## Conclusion

The Yb(III) complexes are prepared from $Yb(NO_3)_3 \cdot 6H_2O$ and Schiff-base ligands derived from 8-hydroxyquinoline-2-carbaldehyde with four aroylhydrazines including benzoylhydrazine, 2-hydroxybenzoylhydrazine, 4-hydroxybenzoylhydrazine and isonicotinylhydrazine, respectively. X-ray crystal and other structural analyses show that Yb(III) and all four newly synthesized ligands can form a binuclear Yb(III) complex with a 1:1 metal to ligand stoichiometry by octacoordination at the Yb(III) center. Every ligand acts as a dibasic tetradentate ligand, binding to Yb(III) through the phenolate oxygen atom, nitrogen atom of quinolinato unit and the C = N group, $^{-}$O–C = N– group (enolized and deprotonated from O = C–NH– group) of the aroylhydrazine side chain. Dimerization of this monomeric unit occurs through the phenolate oxygen atoms leading to a central four-membered $(YbO)_2$ ring. It is the key roles of enolization and deprotonation of O = C–NH– group changing into $^{-}$O–C = N– of the aroylhydrazine side chain that the dimeric centronucleus of every Yb(III) complex is of neutral charge, which will afford an efficient route for investigators to well design favorable molecules. In addition, all the ligands and Yb(III) complexes can bind to CT-DNA through intercalations with the binding constants at $10^5$–$10^7$ $M^{-1}$, but Yb(III) complexes present stronger affinities to DNA than ligands. EtBr–DNA fluorescent tracer methods show that all the ligands and Yb(III) complexes can be used as potential anticancer drugs but the antitumor activities of Yb(III) complexes may be better than those of ligands. However, their pharmacodynamical, pharmacological and toxicological properties should be further studied in vivo.

On the other hand, all the ligands and Yb(III) complexes have strong abilities of antioxidation for

hydroxyl radicals and superoxide radicals but Yb(III) complexes show stronger scavenging effects for hydroxyl radicals than ligands. Whether Yb(III) complexes or ligands containing active phenolic hydroxy groups present stronger abilities of scavenging effects for hydroxyl radicals than others. Endowed with antioxidative properties, these DNA binders may be effective inhibitors of the formation of a DNA/TBP complex topoisomerases, which should be studied further in vivo. Moreover, the complex **2c** has lower ability of scavenging superoxide radicals than other complexes and the different mechanism between scavenging hydroxyl radicals and superoxide radicals should be also studied further.

## Supplementary data

Supplementary data associated with this article can be found in the online version. CCDC No.713873 and 713874 contain the supplementary crystallographic data for this paper. These data can be obtained free of charge from The Cambridge Crystallographic Data Centre via www.ccdc.cam.ac.uk/data_request/cif.

**Acknowledgments** The study was supported by the National Natural Science Foundation of China (20475023) and Gansu NSF (3ZS 041-A25-016).

## References

Albrecht M, Osetska O, Fröhliich R (2005) 2-[(8-Hydroxyquinolinyl)methylene]hydrazinecarboxamide: expanding the coordination sphere of 8-hydroxyquinoline for coordination of rare-earth metal (III) ions. Dalton Trans 23:3757–3762. doi:10.1039/b507621h

Ames BN, Shigenaga MK, Hagen TM (1993) Oxidants, antioxidants, and the degenerative diseases of aging. Proc Natl Acad Sci USA 90:7915–7922. doi:10.1073/pnas.90.17.7915

Ayar A, Mercimek B (2006) Interaction of nucleic acid bases and nucleosides with cobalt ions immobilized in a column system. Process Biochem 41:1553–1559

Bagatolli LA, Kivatinitz SC, Fidelio GD (1996) Interaction of small ligands with Human serum albumin IIIA subdomain. How to determine the affinity constant using an easy steady state fluorescent method. J Pharm Sci 85:1131–1132

Baldini M, Belicchi-Ferrari M, Bisceglie F, Pelosi G, Pinelli S, Tarasconi P (2003) Cu(II) complexes with heterocyclic substituted Thiosemicarbazones: the case of 5-Formyluracil synthesis, characterization, X-ray structures, DNA interaction studies, and biological activity. Inorg Chem 42:2049–2055

Barton JK, Danishefsky AT, Goldberg JM (1984) Tris(phenanthroline)ruthenium(II): stereoselectivity in Binding to DNA. J Am Chem Soc 106:2172–2176

Barton JK, Goldberg JM, Kumar CV, Turro NJ (1986) Binding modes and base specificity of tris(phenanthroline) ruthenium(II) enantiomers with nucleic acids: tuning the stereoselectivity. J Am Chem Soc 108:2081–2088. doi:10.1021/ja00268a057

Behrens C, Harrit N, Nielsen PE (2001) Synthesis of a Hoechst 32258 analogue amino acid building block for direct incorporation of a fluorescent, high-affinity DNA binding motif into peptides. Bioconjugate Chem 12:1021–1027

Berezhkovskiy LM, Astafieva IV, Cardoso C (2002) Analysis of peptide affinity to major histocompatibility complex proteins for the two-step binding mechanism. Anal Biochem 308:239–246

Chaires JB, Dattagupta N, Crothers DM (1982) Studies on interaction of anthracycline antibiotics and deoxyribonucleic acid: equilibrium binding studies on the interaction of daunomycin with deoxyribonucleic acid. Biochemistry 21:3933–3940. doi:10.1021/bi00260a005

Chen XM, Cai JW (2003) Single-crystal structural analysis. Principles and practices. Science Press, Beijing

Chen AY, Yu C, Gatto B, Liu LF (1993) DNA minor groove-binding ligands: a different class of mammalian DNA topoisomerase I inhibitors. Proc Natl Acad Sci USA 90:8131–8135. doi:10.1073/pnas.90.17.8131

Chiang SY, Welch J, Rauscher FJ, Beerman TA (1994) Effects of minor groove binding drugs on the interaction of TATA box binding protein and TFIIA with DNA. Biochemistry 33:7033–7040. doi:10.1021/bi00189a003

El-Asmy AA, El-Sonbati AZ, Ba-Issa AA, Mounir M (1990) Synthesis and properties of 7-formyl-8-hydroxyquinoline and its transition metal complexes. Transit Met Chem 5:222–225. doi:10.1007/BF01038379

Frau S, Bernadou J, Meunier B (1997) Nuclease activity and binding characteristics of a cationic "Manganese porphyrin-bis(benzimidazole) dye (Hoechst 33258)" conjugate. Bioconjugate Chem 8:222–231

Geary WJ (1971) The use of conductivity measurements in organic solvents for the charaterisation of coordination compounds. Coord Chem Rev 7:81–122

Guo ZY, Xing RE, Liu S, Yu HH, Wang PB, Li CP, Li PC (2005) The synthesis and antioxidant activity of the Schiff bases of chitosan and carboxymethyl chitosan. Bioorg Med Chem Lett 15:4600–4603. doi:10.1016/j.bmcl.2005.06.095

Hecht SM (1986) The chemistry of activated bleomycin. Acc Chem Res 19:383–391. doi:10.1021/ar00132a002

Hodnett EM, Dunn WJ (1972) Cobalt derivatives of Schiff bases of aliphatic amines as antitumor agents. J Med Chem 15:339. doi:10.1021/jm00273a037

Hodnett EM, Mooney PD (1970) Antitumor activities of some Schiff bases. J Med Chem 13:786. doi:10.1021/jm00298a065

Horton AA, Fairhurst S (1987) Lipid peroxidation and mechanisms of toxicity. Crit Rev Toxicol 18:27–29. doi:10.3109/10408448709089856

Hunter RB, Walker W (1956) Anticoagulant action of Neodymium 3-Sulpho-isonicotinate. Nature 178:47. doi:10.1038/178047a0

Ismail TMA (2005) Mononuclear and binuclear Co(II), Ni(II), Cu(II), Zn(II) and Cd(II) complexes of Schiff-base ligands derived from 7-formyl-8-hydroxyquinoline and diaminonaphthalenes. J Coord Chem 58:141–151

Kramsch DM, Aspen AJ, Rozler LJ (1981) Atherosclerosis: prevention by agents not affecting abnormal levels of blood lipids. Science 213:1511–1512. doi:10.1126/science.6792706

Krishna AG, Kumar DV, Khan BM, Rawal SK, Ganesh KN (1998) Taxol–DNA interactions: fluorescence and CD studies of DNA groove binding properties of taxol. Biochim Biophys Acta 1381:104–112

Li ZL, Chen JH, Zhang KC, Li ML, Yu RQ (1991) Fluorescent study on the primary screening for nonplatinum type of Schiff-base antitumor complexes. Science in China Series B: Chemistry 11:1193–1200

Lippard SJ (1978) Platinum complexes: probes of polynucleotide structure and antitumor drugs. Acc Chem Res 11:211–217. doi:10.1021/ar50125a006

Liu YC, Yang ZY, Du J, Yao XJ, Lei RX, Zheng XD, Liu JN, Hu HS, Li H (2008) Study on the interactions of Kaempferol and Quercetin with intravenous immunoglobulin by fluorescence quenching, Fourier transformation infrared spectroscopy and circular dichroism spectroscopy. Chem Pharm Bul 56:443–451

Lo SF, Mulabagal V, Chen CL, Kuo CL, Tsay HS (2004) Bioguided fractionation and isolation of free radical scavenging components from in vitro propagated Chinese medicinal plants *Dendrobium tosaense* Makino and *Dendrobium moniliforme* SW. J Agric Food Chem 52:6916–6919. doi:10.1021/jf040017r

Lu XH, Lin QY, Kong LC, He XQ (2006) Synthesis of binuclear rare earth complexes of N, N′-bis(2-pyridinecarboxamide)-1, 2-ethane and study on their Interaction with deoxyribonucleic acid. Chem Res Appl 18: 1380–1385

Lu HL, Liang JJ, Zeng ZZ, Xi PX, Liu XH, Chen FJ, Xu ZH (2007) Three salicylaldehyde derivative Schiff base $Zn^{II}$ complexes: synthesis, DNA binding and hydroxyl radical scavenging capacity. Transit Metal Chem 32:564–569

Mahadevan S, Palaniandavar M (1997) Spectroscopic and voltammetric studies of copper(II) complexes of bis(pyrid-2-yl)-di/trithia ligands bound to calf thymus DNA. Inorg Chim Acta 254:291–302. doi:10.1016/S0020-1693(96)05175-4

McGhee JD, von Hippel PH (1974) Theoretical aspects of DNA-protein interactions: co-operative and non-co-operative binding of large ligands to a one-dimensional homogeneous lattice. J Mol Biol 86:469–489. doi:10.1016/0022-2836(74)90031-X

Moawad MM, Hanna WG (2002) Structural and antimicrobial studies of some divalent transition metal complexes with some new symmetrical bis(7-formylanil substituented-sulfoxine) Schiff base ligands. J Coord Chem 55:439–457

Ou-Yang JM (1997) Synthesis properties and characterization of the complexes of 2-(N-hexadecylcarbamoyl)-8-hydroxyqunoline. J Inorg Chem 13:315–319

Palchaudhuri R, Hergenrother PJ (2007) DNA as a target for anticancer compounds: methods to determine the mode of binding and the mechanism of action. Curr Opin Biotechnol 18:497–503

Parker D, Dickins RS, Puschmann H, Crossland C, Howard JAK (2002) Being excited by lanthanide coordination complexes: aqua species, chirality, excited-state chemistry, and exchange dynamics. Chem Rev 102:1977–2010. doi:10.1021/cr010452+

Pyle AM, Morii T, Barton JK (1990) Probing microstructures in double-helical DNA with chiral metal complexes: recognition of changes in base-pair propeller twisting in solution. J Am Chem Soc 112:9432–9434. doi:10.1021/ja00181a077

Satyanarayana S, Dabrowiak JC, Chaires JB (1992) Neither Δ- nor Λ-Tris(phenanthroline)ruthenium(II) Binds to DNA by classical intercalation. Biochemistry 31:9319–9324. doi:10.1021/bi00154a001

Scatchard G (1949) The attractions of protein for small molecules and ions. Ann N Y Acad Sci 51:660–673. doi:10.1111/j.1749-6632.1949.tb27297.x

Schmidt LH (1969) Chemotherapy of the drug-resistant malarias. Annu Rev Microbiol 23:427–454. doi:10.1146/annurev.mi.23.100169.002235

Sheldrick GM (1990) Phase annealing in SHELX-90: direct methods for larger structures. Acta Crystallogr A 46:467–473. doi:10.1107/S0108767390000277

Sigman DS, Mazumder A, Perrin DM (1993) Chemical nucleases. Chem Rev 93:2295–2316

Snyder RD (2007) Assessment of atypical DNA intercalating agents in biological and in silico systems. Mutat Res 623:72–82

Suh D, Chaires JB (1995) Criteria for the mode of binding of DNA binding agents. Bioorg Med Chem 3:723–728. doi:10.1016/0968-0896(95)00053-J

Ueda J-i, Saito N, Shimazu Y, Ozawa T (1996) A comparison of scavenging abilities of antioxidants against hydroxyl radicals. Arch Biochem Biophys 333:377–384

Wang Y, Yang ZY, Wang Q, Cai QK, Yu KB (2005) Crystal structure, antitumor activities and DNA-binding properties of the La(III) complex with Phthalazin-1(2H)-one prepared by a novel route. J Organomet Chem 690:4557–4563

Wang HL, Yang ZY, Wang BD (2006) Synthesis, characterization and the antioxidative activity of copper(II), zinc(II) and nickel(II) complexes with naringenin. Transit Met Chem 31:470–474. doi:10.1007/s11243-006-0015-3

Wang BD, Yang ZY, Crewdson P, Wang DQ (2007) Synthesis, crystal structure and DNA-binding studies of the Ln(III) complex with 6-hydroxychromone-3-carbaldehyde benzoyl hydrazone. J Inorg Biochem 101:1492–1504. doi:10.1016/j.jinorgbio.2007.04.007

Winterbourn CC (1979) Comparison of superoxide with other reducing agents in the biological production of hydroxyl radicals. Biochem J 182:625–628

Winterbourn CC (1981) Hydroxyl radical production in body fluids. Roles of metal ions, ascorbate and superoxide. Biochem J 198:125–131

Woynarowski JM, Mchugh M, Sigmund RD, Beerman TA (1989) Modulation of Topoisomerase II catalytic ativity by DNA minor groove binding agents distamycin,

Hoechst 33258 and 4′, 6-Diamidine-2-phenylindole. Mol Pharmacol 35:177–182

Wu JZ, Ye BH, Wang L, Ji LN, Zhou JY, Li RH, Zhou ZY (1997) Bis(2, 2'-bipyridine)ruthenium(II) complexes with imidazo[4, 5-f][1, 10]-phenanthroline or 2-phenylimidazo[4, 5-f][1, 10]phenanthroline. J Chem Soc Dalton Tran 8:1395–1402

Xing R, Yu H, Liu S, Zhang W, Zhang Q, Li Z, Li P (2005) Antioxidant activity of differently regioselective chitosan sulfates in vitro. Bioorg Med Chem 13:1387–1392

Yang MM, Yang P, Zhang LW (1994) Study on interaction of caffeic acid series medicine and albumin by fluorescence method. Chin Sci Bull 9:31–36

Zeng YB, Yang N, Liu WS, Tang N (2003) Synthesis, characterization and DNA-binding properties of La(III) complex of chrysin. J Inorg Biochem 97:258–264. doi: 10.1016/S0162-0134(03)00313-1

Zsila F, Bikádi Z, Simonyi M (2004) Circular dichroism spectroscopic studies reveal pH dependent binding of curcumin in the minor groove of natural and synthetic nucleic acids. Org Biomol Chem 2:2902–2910. doi: 10.1039/b409724f